

# Viewing spin structures with soft X-ray microscopy

The spin of the electron and its associated magnetic moment marks the basic unit for magnetic properties of matter<sup>1,2</sup>. Magnetism, in particular ferromagnetism and antiferromagnetism is described by a collective order of these spins, where the interaction between individual spins reflects a competition between exchange, anisotropy and dipolar energy terms. As a result the energetically favored ground state of a ferromagnetic system is a rather complex spin configuration, the magnetic domain structure<sup>3</sup>. Magnetism is one of the eldest scientific phenomena, yet it is one of the most powerful and versatile utilized physical effects in modern technologies, such as in magnetic storage and sensor devices. To achieve highest storage density, the relevant length scales, such as the bit size in disk drives is now approaching the nanoscale and as such further developments have to deal with nanoscience phenomena<sup>4-9</sup>. Advanced characterization tools are required to fully understand the underlying physical principles. Magnetic microscopes using polarized soft X-rays offer a close-up view into magnetism with unique features, these include elemental sensitivity due to X-ray magnetic dichroism effects as contrast mechanism, high spatial resolution provided by state-of-the-art X-ray optics and fast time resolution limited by the inherent time structure of current X-ray sources, which will be overcome with the introduction of ultrafast and high brilliant X-ray sources.

Peter Fischer

Center for X-ray Optics, E.O. Lawrence Berkeley National Laboratory, 1, Cyclotron Road, Berkeley CA 94720 U.S.A.

E-mail: [PJFischer@lbl.gov](mailto:PJFischer@lbl.gov)

The primary goal of magnetic microscopies is to image the static domain structure, i.e. the spin configuration in thermal equilibrium viewed at highest spatial resolution. A large variety of magnetic imaging techniques has been developed which are available to study magnetic systems. They can be classified to the probes they use. There are optical microscopes using the magneto-optical Kerr effect (MOKE), where a contrast is generated by the rotation of the polarization vector of the incoming light by a magnetic moment; there are electron microscopes, such as the Lorentz transmission electron microscope (TEM), which utilizes the Lorentz force diverting the electrons as they propagate through the magnetic specimen<sup>10,11</sup>, or the Scanning Electron Microscope with subsequent Polarization Analysis of the electrons (SEMPA)<sup>12</sup>. There are also several scanning probe microscopes, such as the Magnetic Force Microscope (MFM), which senses the interaction of the stray field emanating from the sample onto its magnetic tip or the Spin Polarized Scanning Tunneling Microscope (SP-STM), which detects the tunneling current between the atomic tip and the sample's surface<sup>13,14</sup>. Among magnetic microscopy techniques the SP-STM leads in spatial resolution as it has so far achieved almost atomic resolution. Whereas Kerr microscopy is diffraction limited in its spatial resolution, by using ultrafast laser systems, it can study ultrafast spin dynamics down to fsec time scales<sup>15,16</sup>. Studies of ultrafast spin dynamics have gained significant interest in the recent past, since ultimately the temporal evolution of spin structures provides insight into the basic mechanism of the magnetic interactions and also determines the functionalities of magnetic devices.

There are several ways to control magnetization on a nanoscale. The traditional mechanism is to apply an external magnetic field, which goes back to the more than 150 year old experiments by Oersted, but is still the technique of choice to write for example information in a magnetic hard drive<sup>17</sup>. However, this mechanism runs into inherent limitations when the characteristic feature sizes approach the nanoscale. The long ranging dipolar field has a strong impact to neighboring cells, leading to significant cross-talk problems in devices. Further, the writing speed, i.e. the reversal of the magnetic moment as the external field is pointing in opposite direction to the moment is relatively slow, since the torque exerted on the moment is small and relies on thermal fluctuations of the magnetic moment to initiate the reversal process. Finally, there is the problem of the superparamagnetic limit<sup>18</sup>, which requires on one hand high anisotropy media to compensate the counteracting spontaneous (Boltzmann) driven reversal, which on the other hand requires strong magnetic fields acting on short length scales, which is technologically very challenging to realize.

In addition to the charge of the electron the concept of spintronics considers also its spin as a new degree of freedom<sup>18-30</sup>. This opens new avenues to manipulate spins on the nanoscale<sup>31</sup>. By injecting a

spin polarized current into a ferromagnet, a torque is exerted onto a non-uniform spin configuration in the system, which can reverse the magnetization<sup>32</sup>, move a domain wall<sup>33</sup> or excite the dynamics of a vortex core<sup>34-36</sup>. This spin torque effect scales in a more favorable way than the Oersted field since its efficiency increases with decreasing length scale. Another exciting possibility is to manipulate ferromagnetism by electric fields only. This is the thrust of multiferroic materials, which combine ferroelectric and ferromagnetic properties<sup>37-40</sup>. Whereas this is scientifically a very fascinating area on its own, multiferroic research is also driven by the fact, that high magnetic fields on short length scales are technically much more challenging to realize and to control than electric fields of similar strengths.

Advanced materials play an ever increasing role in modern magnetism and therefore the design and synthesis of novel magnetic materials with tailored properties has received significant interest recently. Systems with high spin polarization are needed for an efficient spin torque effect and Heusler alloys show great potential<sup>41-46</sup>. Multiferroic hetero-structures are designed with state-of-the-art molecular beam Epitaxy techniques since in nature there is only a very limited number of compounds which exhibit a coexistence of ferromagnetic and ferroelectric order.

Whereas spin torque devices would still require an electron current, there is increased interest in exploring concepts of electronics, which are complete free of charge. If one could use pure spin currents without moving charges, this would lead to new perspectives in electronics, since it would remedy effects such as Joule heating or the need to generate magnetic fields<sup>47-54</sup>.

Both research and technology of nanoscale magnetism has come a long way and fundamental length scales such as magnetic exchange lengths, which are determined by material specific exchange and anisotropy constants are within reach both from the synthesis, analytics and technological point of view<sup>55</sup>. In contrast, current typical magnetization reversal times in the devices are still in the tens of psec regime. This is orders of magnitude away from fundamental time scales in magnetism. They are in the tens of fsec, which relates to the strength of exchange interaction. Nowadays such time scales are experimentally accessible with ultrafast optical laser systems and recent experiments have verified that it is possible to switch a spin configuration with a single fsec polarized laser pulse<sup>56</sup>. This inverse Faraday effect has launched the field of opto-magnetism which offers the opportunity to explore the ultimate speed in reversing magnetic moments. Although the experimental data are convincing and provide important input to the development of theoretical models, a fundamental understanding of the processes involved is still largely missing<sup>57-59</sup>.

Progress in nanomagnetism research depends on the interaction and advancements of three different areas. State-of-the-art synthesis of materials exhibiting novel magnetic functionality has to be

accompanied by both cutting edge analytical tools and theoretical modeling.

The availability of circularly polarized soft X-rays and the capability to utilize magnetic dichroism effects<sup>60</sup> has launched a wealth of powerful spectroscopic and microscopic tools<sup>61</sup>. Various microscopy techniques have evolved, which allow to image with elemental specificity, high spatial and temporal resolution spin structures and their fast dynamics in a multitude of nanoscale magnetic system, such as thin films, hetero-structures, alloys or nanostructures. X-ray magnetic circular dichroism (X-MCD) is the effect, that the absorption of circularly polarized X-rays having a photon energy close to species specific inner core binding energies depends strongly on the relative orientation between the photon helicity and the projection of the magnetic moments onto the photon propagation direction. X-MCD can be seen as the X-ray counterpart to the optical Kerr effect. It can yield values up to tens of percent and provides the inherent element-specificity and strong magnetic contrast for magnetic X-ray imaging techniques.

The first X-ray microscopy results utilized a X-ray photoemission electron microscope (X-PEEM)<sup>62</sup>. It detects the secondary photoelectrons generated in the X-ray absorption process and images them through an electron microscopy optics onto a 2-dimensional detector. The limited escape depth of photoelectrons makes this technique suited to study surfaces. Complementary to X-PEEM are X-ray microscopies which use X-ray imaging optics<sup>63,64</sup>. Since the refractive index of X-rays is close to unity, conventional lenses do not work, however, Fresnel zone plates (FZP), which are circular gratings with a radially increasing line density, allow for focusing X-rays. They can be fabricated by state-of-the-art lithography techniques and their performance can be designed by choosing a few parameters,

such as the outermost zone width  $\Delta r$ , the number of zones  $N$  and the wavelength they are working at, which determines e.g. the achievable focal length and spatial resolution.

There are two types, a scanning transmission X-ray microscope (STXM) and a full field imaging transmission X-ray microscope (TXM). The optical setup of the full field soft X-ray microscope beamline XM-1 located at the Advanced Light Source in Berkeley CA is shown in Fig. 1<sup>65</sup>. Its optical design is similar to a conventional optical microscope. A bending magnet in the synchrotron provides the X-rays, which are elliptically polarized above and below the orbital plane. A condenser zone plate (CZP) and a small pinhole close to the sample provides a hollow cone illumination of a small band of X-rays. After transmitting the sample, a second FZP, the micro zone plate (MZP) generates the high resolution image, which is recorded by a 2dimensional charge-coupled device (CCD) detector. The first magnetic X-ray microscopy image with a zone plate based TXM was published in 1996 using X-MCD as strong magnetic contrast<sup>66</sup>. Since both TXM and STXM<sup>67</sup> detect the X-rays transmitted through the sample, they are sensitive to the bulk properties, which complements the X-PEEM technique. However, as pure photon techniques they can record images of spin structures while external magnetic fields are applied, which is very difficult for electron based microscopies.

### Advances in X-ray optics

The most recent advances in Fresnel zone plate fabrication can be seen in Fig. 2<sup>68</sup>, where test patterns of dense Si/Mo lines and spaces could be imaged with XM-1 down to better than 12nm spatial resolution. This was possible by developing a new nanofabrication process for the zone plate. It is based on a double patterning technique (see sketch in Fig. 2<sup>68</sup>). The challenge in preparing high resolution and

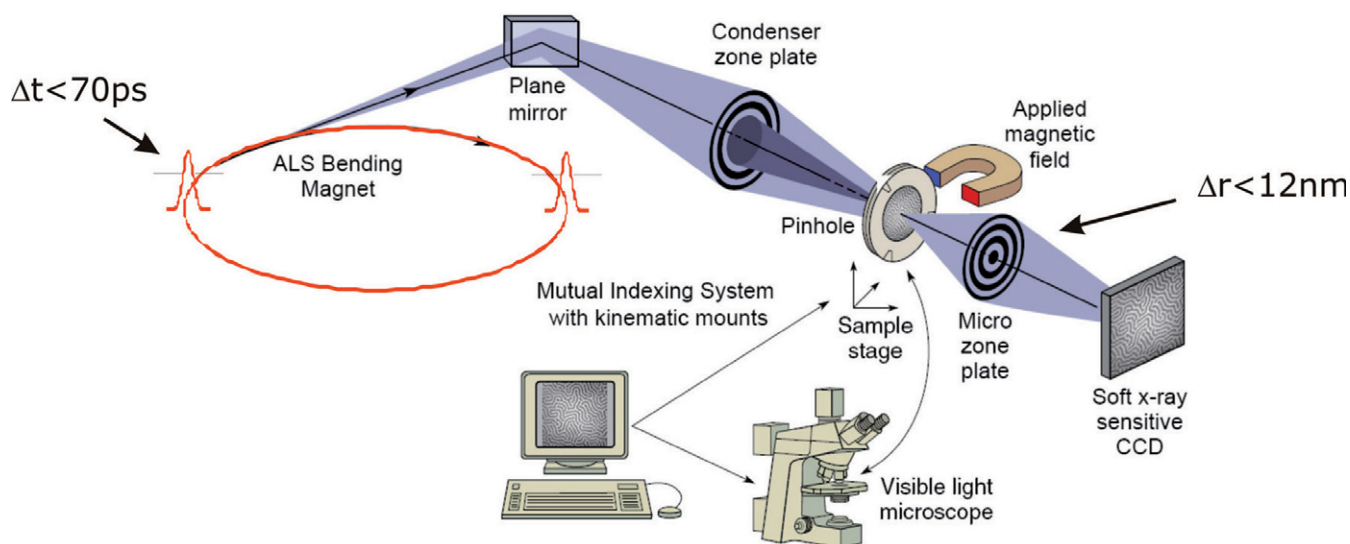


Fig. 1 X-ray optical set-up of the full field X-ray microscope XM-1 at the Advanced Light Source In Berkeley CA. A condenser zone plate and a pinhole provide a hollow cone illumination of the X-ray flashes (duration <70ps) emitted from a bending magnet onto the sample. The micro zone plate, i.e. the X-ray objective lens (spatial resolution <12nm) projects a magnified image from the transmitted X-rays onto the CCD detector. Reproduced with permission from<sup>65</sup>.

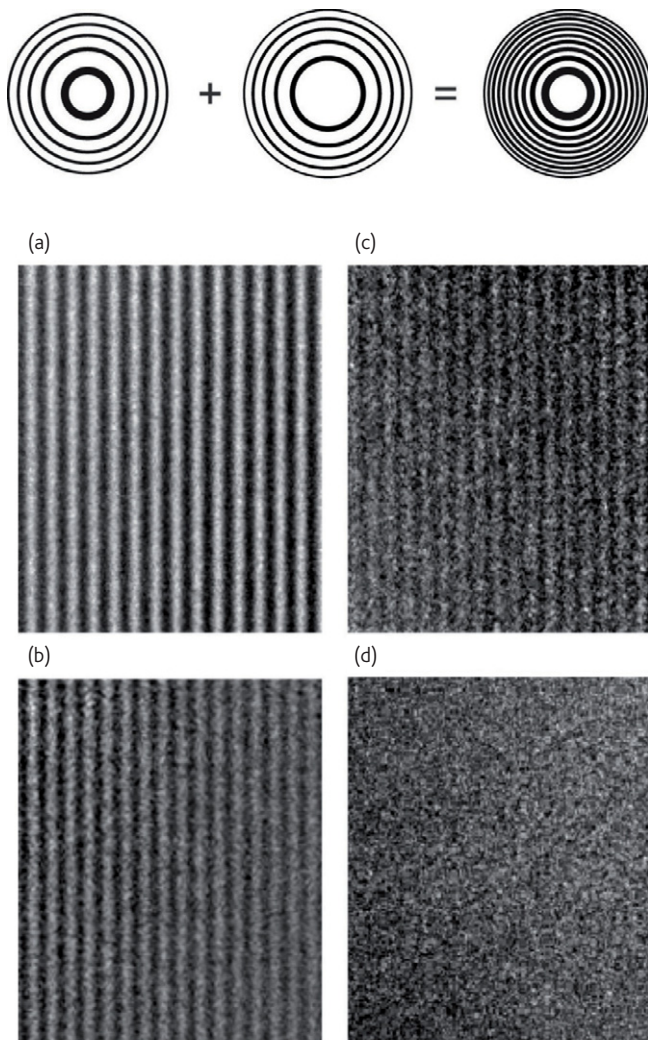


Fig. 2 Top: Schematics of the overlay technique to fabricate high resolution X-ray optics. Bottom: X-ray microscopy images of Mo/Si test patterns obtained with a 12 nm micro zone plate at 707eV photon energy. The patterns have half-periods of (a) 20 nm, (b) 15 nm, (c) 12 nm, and (d) 10 nm. Reproduced with permission from<sup>68</sup>.

high efficient zone plates is to generate a dense circular line pattern with a sufficiently high aspect ratio. Instead of performing the process in a single step, a new process splits the task into two subtask each generating a subpattern with a not-so-dense line pattern. After the first sub pattern is generated, in a second step the second half of the zone plate is fabricated by placing the remaining lines at their accurate positions. This requires a high placement accuracy for the e-beam lithography, which can be achieved using sophisticated optimization algorithms.

In the following some recent examples with magnetic soft X-ray microscopy are presented, which demonstrate the achievements and capabilities of this analytical tool to study challenging problems in nanomagnetism. Of particular interest are spin structures of nanoscale dimension.

### Stochastic behavior on the nanoscale

The basic question whether magnetic processes behave deterministically on a nanoscale is both scientifically interesting, but in view of current developments towards storage media with higher density also of paramount technological interest.

The field driven reversal of magnetic materials is known to occur via a series of discrete and sudden jumps in the magnetization, which are the Barkhausen avalanches<sup>69</sup>. Studies have revealed a power-law scaling behavior of the Barkhausen avalanches<sup>70,71</sup>, which connects them to a wide variety of physical phenomena, such as metal-insulator transitions, earthquakes, vortices in superconductors or charge density waves<sup>72-75</sup>. The scaling exponent is a characteristic parameter, which is also studied theoretically. Fig. 3<sup>76</sup> shows the results of an X-ray microscopy study at better than 15nm spatial resolution of the Barkhausen avalanche process and its scaling behavior in a CoCrPt nanogranular thin film with a pronounced perpendicular magnetic anisotropy. Such systems are discussed as perpendicular magnetic recording media. The average grain size of the system studied was determined to be around 20nm<sup>77</sup>, therefore the X-ray microscopy results provide information at the fundamental grain level. The jump of domain size at each field step throughout the full hysteresis loop was measured and analyzed. Power law scaling behavior with a constant exponent close to unity was found at all field steps but close to coercivity, where a sudden jump of the exponent to 1.5 was observed. This indicates that a proximity effect has a large impact to the Barkhausen avalanches in these systems<sup>76</sup>.

Magnetic domain walls, which separate two domains of opposite magnetization direction are discussed as basic units in novel concepts for magnetic storage, such as the racetrack memory<sup>78</sup>, where domain walls are pushed along magnetic nanowires by injecting short electronic pulses. And even novel concepts for magnetic logic elements are considered which are based on magnetic domain walls<sup>79</sup>.

A recent X-ray microscopy study focused on exploring the reliability of domain wall motion in magnetic nanowires<sup>80</sup>. Small notches were fabricated by lithography into ferromagnetic nanowires which act as a pinning site for the domain walls. The propagation was observed as the external field was increased. Fig. 4<sup>80</sup> shows a sample of images of the various geometries of the wires and the fields which were applied. This study clearly revealed a strong stochastic component in the depinning and pinning process. It turned out that it depends strongly on the geometry of the wire and the notches and therefore a proper choice of the wire geometry allows to control the non-deterministic character of this process.

### Current driven domain walls

In view of the application of domain walls, their dynamics particular when driven by spin torque is of paramount interest<sup>81-83</sup>. In Fig. 5a<sup>84</sup> a schematic of an infinity shaped permalloy (a NiFe alloy) element is shown which was fabricated to obtain time resolved X-ray

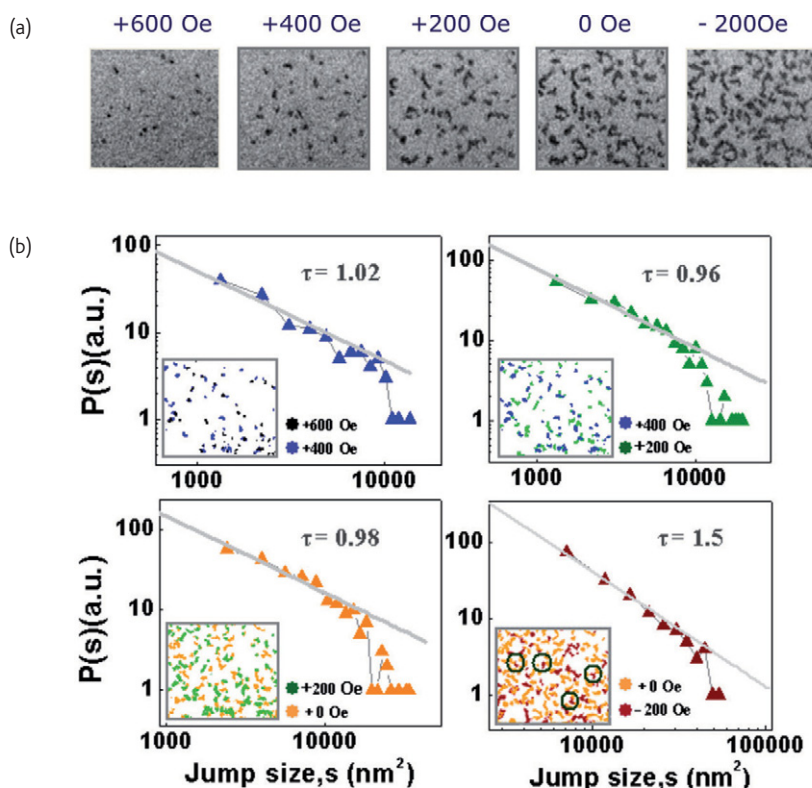


Fig. 3 Top: M-TXM images recorded at 15nm spatial resolution of the domain evolution of a in  $(\text{Co}_{0.83}\text{Cr}_{0.17})_{87}\text{Pt}_{13}$  alloy film as function of applied magnetic field. Bottom: Distributions of the Barkhausen avalanche size taken at field steps along the hysteresis loop. The inset images are superimposed domain configurations taken at the initial and final fields of each step. The scaling exponent is close to 1 apart from coercivity, where it jumps to 1.5 as a result of proximity. Reproduced with permission from<sup>76</sup>.

microscopy images of a domain wall trapped between the open holes of the element. From the electric contact pads above and below the element, short electronic pulses were injected to excite the domain wall dynamics. Fig. 5b<sup>84</sup> shows the static spin configuration with the domain wall in the center of the infinity shape.

A stroboscopic pump-probe scheme is used for time resolved X-ray microscopy, where the X-ray probe pulses are delayed relative to the electrical pump pulses<sup>84</sup>. Fig 5c shows the analysis of the observed domain wall dynamics. After the pump pulse the domain wall is deflected and oscillates around the static position ( $y=0\text{nm}$ ) for several

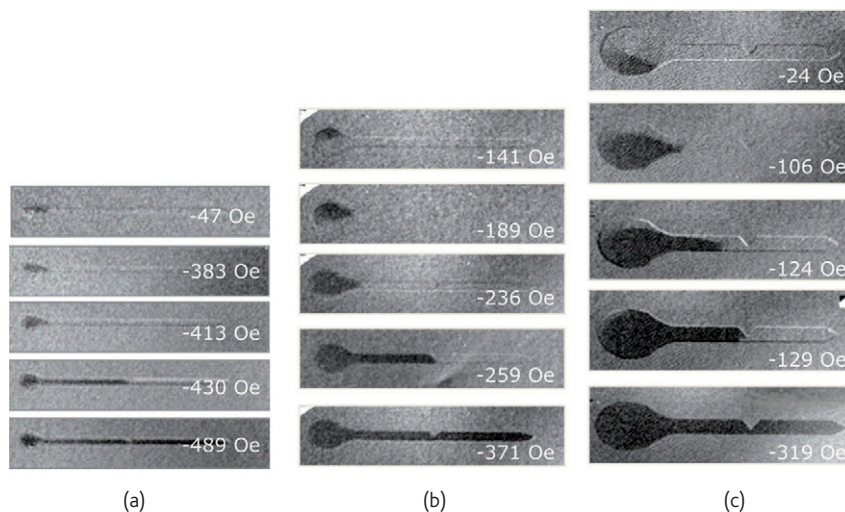


Fig. 4 Three representative image sequences of magnetic domain-wall evolution along the hysteresis cycle for wire widths of  $w = 150 \text{ nm}$  (a),  $250 \text{ nm}$  (b), and  $450 \text{ nm}$  (c). The magnetic field of thDW domain wall evolution pattern is indicated. Reproduced with permission from<sup>80</sup>.

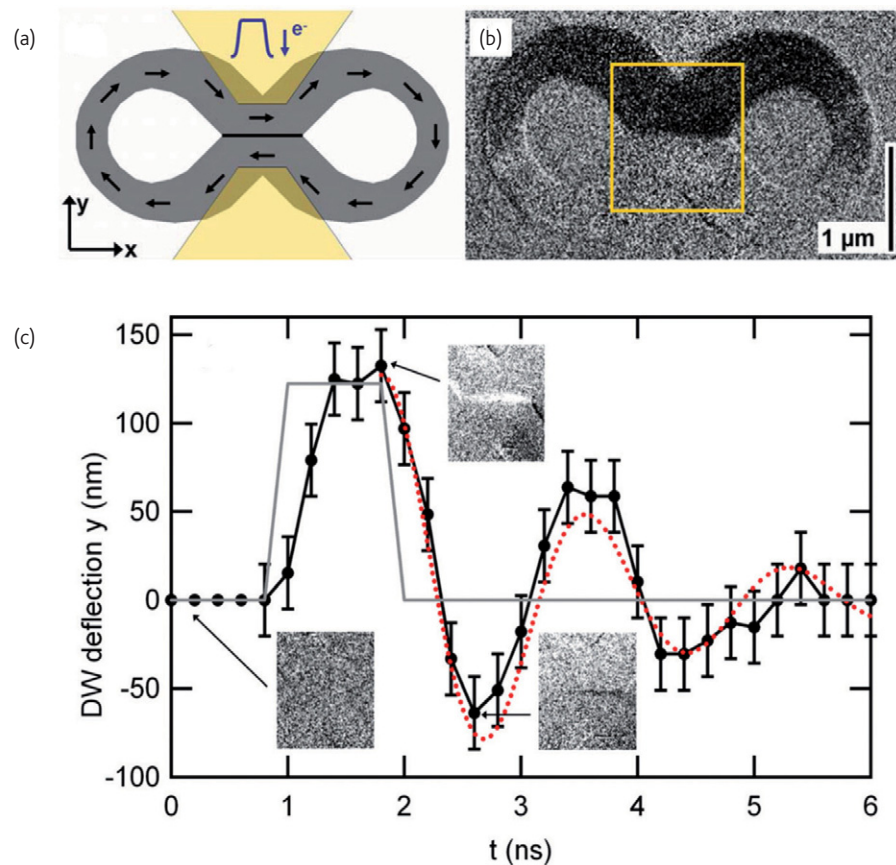


Fig. 5 (a) Scheme of the infinity structure and its magnetization (arrows). The Au contact pads are marked as yellow areas. (b) Differential x-ray image showing the static magnetic configuration with the domain wall in the center. (c) Time evolution of the vertical deflection of the DW domain wall. The gray curve depicts the current pulse. The dotted red curve is a fit to the free oscillation. The inset images show differential x-ray images of the deflection of the domain wall at 200, 1800, and 2600 ps delay time. The horizontal white structure at 1800 ps indicates that the domain wall has moved upwards, while the corresponding black horizontal structure at 2400 ps reflects that the domain wall has moved down, but with less amplitude. Reproduced with permission from<sup>84</sup>.

periods which extends up to several nanoseconds. The insets in Fig. 5c are typical experimental difference images, where a bright contrast represents a positive deflection. These results could be fully explained within an analytical model, which had to take into account higher than harmonic orders in the pinning potential.

### Cell trapping with domain walls

So far, magnetic domain walls have been considered as nanoscale non-uniform magnetic spin structures. However, they also can act as a localized sources of strong magnetic fields. As such they can be considered as trapping sites for beads, which in turn could attach to cells. This would open now the possibility to control through the manipulation of the domain wall by a magnetic field a cell, e.g. it could be used as a nanoscale cell trapping device. One can envision to move the cell by either magnetic fields and current pulses. To this end a recent soft X-ray microscopy study was performed to image the manipulation of domain walls in certain ferromagnetic structures. Of particular interest is the switch configuration, which can be easily

altered by applying magnetic field. Fig. 6 shows first results of the X-ray microscopy study of the domain structure occurring for this mechanism. The forces can easily be obtained from analytical formula and simulations agree well with experimental observations<sup>85</sup>.

### Vortex dynamics

Magnetic vortex structures occur in confined elements. They consist of a circulating in-plane magnetization, with a vortex core in the center, where the magnetization as a result of competing exchange and dipolar fields points perpendicular to the plane of the disk. Vortex structures are the energetic ground state in small disks of permalloy and particularly their vortex core is considered for storage applications because of its stable spin configuration<sup>86</sup>.

Magnetic vortex cores have been imaged with a variety of microscopy techniques, including MFM<sup>87</sup>, which was able to detect the direction of the stray field generated in the vortex core and also SP-STM, which has studied the static vortex core with unprecedented spatial resolution<sup>88,89</sup>. Fig. 7a shows the magnetic vortex cores in

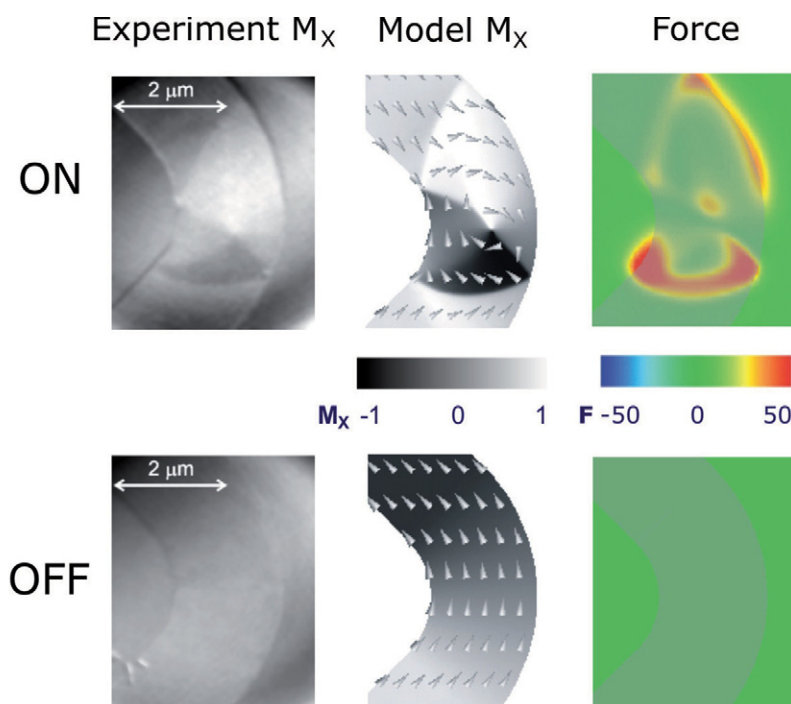


Fig. 6 Left: X-ray microscopy of the domain configuration for the ON/OFF switch settings. Center: Micromagnetic simulations of the domain configuration. Right: Calculate magnetic force for the ON/OFF switch settings. Reproduced with permission from<sup>85</sup>.

500nm radius permalloy disk structure, as obtained from state-of-the-art full field X-ray microscopy, and a 3-dimensional representation derived from the X-ray microscopy images is shown in Fig. 7b.

Again, the dynamics of magnetic vortex structures has gained significant interest. Vortex dynamics, if excited by spin current pulses, can be used to determine the polarization of the currents, which in fact quantifies the strength of the spin torque effect. The

results of a recent time resolved X-ray microscopy studies are shown in Fig. 8<sup>90</sup>.

In the upper half of Fig. 8 one sees the experimental stroboscopic pump-probe setup, which was used to measure the gyration radius of the vortex core as a function of resonant excitation frequency. Utilizing the Thiele equation which includes spin transfer terms, it was possible to derive unambiguously the polarization of the currents in permalloy

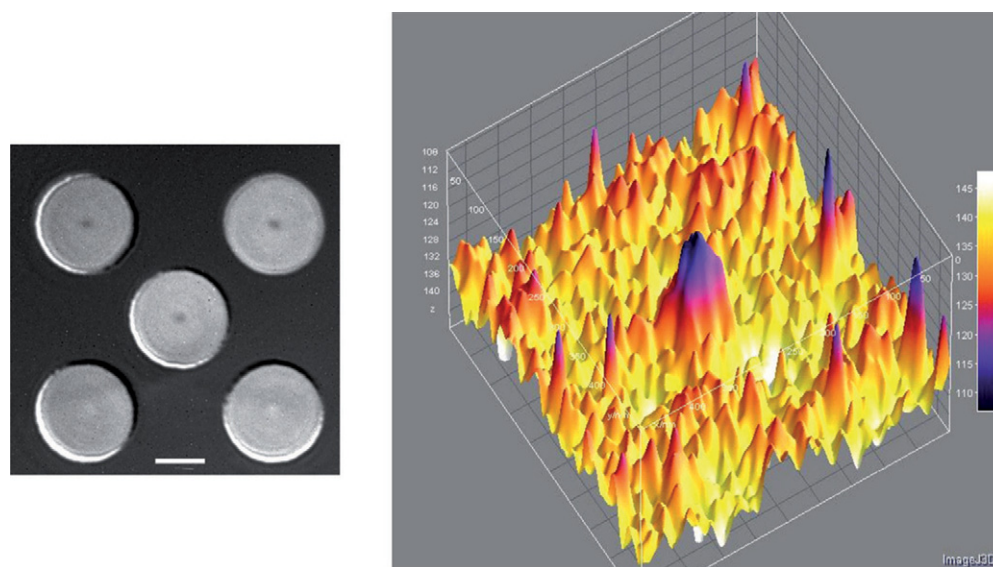


Fig. 7 Left: Magnetic X-ray microscopy image of the Magnetic vortex cores in permalloy disk structures with a radius of 500nm and thickness 150nm. Right: Three dimensional representation of X-ray image of a vortex core in the disk structures

to be 0.67 (see lower part of Fig 8). The results from other techniques to obtain this quantity scattered largely and were often hampered by interface effects or could only indirectly derived<sup>90</sup>.

### Future directions

Progress in X-ray microscopies, particular the (S)TXM instruments benefit tremendously from advances in X-ray optics and the less than 10nm regime is around the corner<sup>91</sup>. The possibility of replication of high quality condenser zone plate is currently being explored in a similar framework as master copies e.g. for bit patterned media<sup>92-94</sup>.

A complementary, but conceptual different approach than using state-of-the-art X-ray optics is pursued in the realm of lensless imaging techniques. The basic idea here is to collect a diffractive or holographic pattern from the specimen under investigation and calculate by sophisticated retrieval algorithms the nanoscale structures in real space<sup>95</sup>. Notable achievements to image e.g. magnetic spin structures have been reported recently<sup>95-97</sup>.

X-ray imaging of spin dynamics on the ultrafast fsec magnetic time scale is waiting for the appropriate high brilliant and ultrafast X-ray sources, which could be either X-ray free electron lasers<sup>98,99</sup> or even lab experiments based on high harmonic generation sources<sup>100,101</sup>. Both the real and the reciprocal imaging techniques need to explore their potential to obtain a close-up snapshot look of spin structures at their fundamental magnetic length and time scales. 

### Acknowledgement

We would like to acknowledge the numerous fruitful and stimulating collaborations, in particular with M.-Y. Im, W. Chao, E. Anderson (CXRO), S.-C. Shin (KAIST Korea), K.-S. Lee, S.-K. Kim (Seoul Natl University), D.-H. Kim (Chungbuk University), G. Meier, L. Bocklage, M. Bolte (U Hamburg), S. Kasai (NIMS Tsukuba), A. Thiaville (U Paris-Sud), M. Bryan, P. Fry, D. Allwood (U Sheffield), S. Mangin (U Nancy). The continuous support of the staff of CXRO and ALS is highly appreciated. This work was supported by the Director, Office of Science, Office of Basic Energy Sciences, of the U.S. Department of Energy.

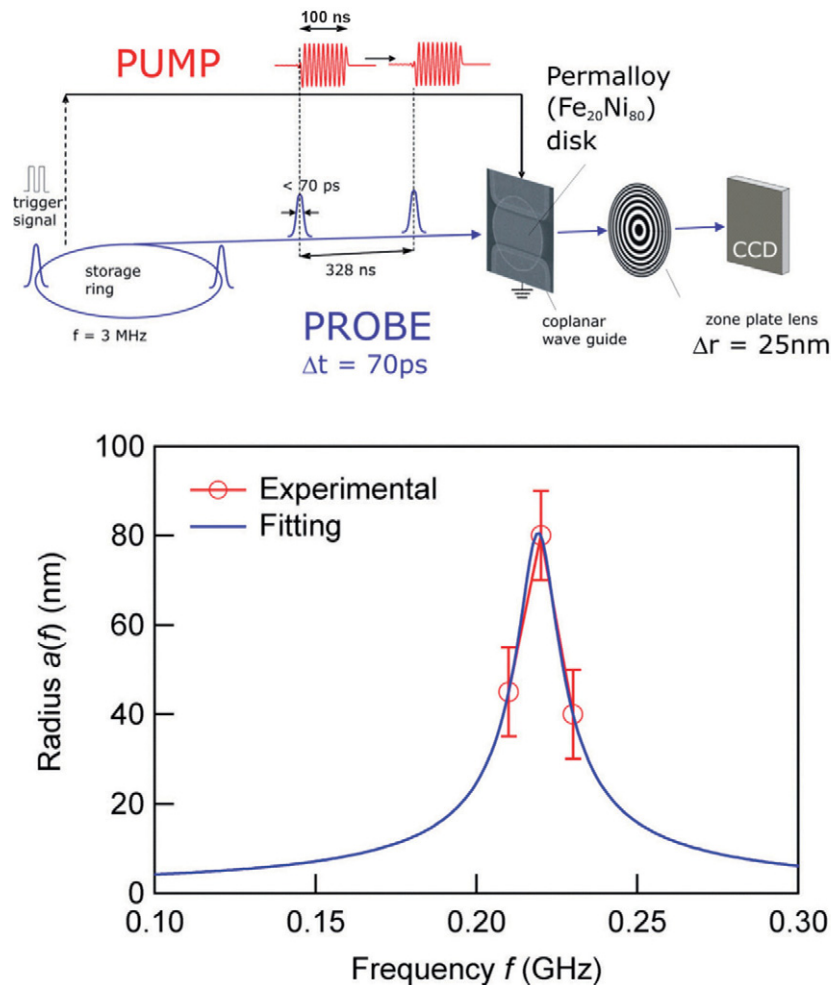


Fig. 8 Top: Schematics of the time resolved pump-probe X-ray microscopy experiment. Bottom: Experimentally observed gyration radius as function of excitation frequency. From a fit of this profile the polarization of the current can be obtained. Reproduced with permission from<sup>90</sup>.

**REFERENCES**

1. Pauli, W., *Z Phys* (1925) **31**, 765.
2. Uhlenbeck, G. E., and Goudsmit, S., *Naturwissenschaften* (1925) **13**, 953; *Nature, London* (1926) **117**, 264.
3. Hubert, A., and Schäfer, R., "Magnetic Domains" (1998) Springer, New York,
4. Bader, S. D., and Parkin, S. S. P., *Annu Rev Condens Matter Phys* (2010) **1**, 3.1-3.18.
5. Chapprt, C., and Kim, J. V., *Nat Phys* (2008) **4**, 837.
6. Marrows, C. H., et al., *Mater Today* (2009) **12** (7-8), 70.
7. Ohno, Y., et al., *Nature* (1999) **402**, 790.
8. Wolf, S. A., et al., *Science* (2001) **294**, 1488.
9. Awschalom, D. D., and Flatte, M. E., *Nat Phys* (2007) **3**, 153.
10. Chapman, J. N., et al., *IEEE Trans Mag* (1990) **26**, 1506.
11. Phatak, C., et al., *Ultramicroscopy* (2009) **109**, 264.
12. Chung, S. H., et al., *Ultramicroscopy* (2010) **110**, 177.
13. Krause, S., et al., *Science* (2007) **317**, 1537.
14. Loth, S., et al., *Nat Phys* (2010) **6**, 340.
15. Park, J. P., et al., *Phys Rev B* (2003) **67**, 020403(R).
16. Acremann, Y., et al., *Science* (2000) **290**, 492.
17. Moser, A., et al., *J Phys D* (2002) **35**, R157.
18. Weller, D., and Moser, A., *IEEE Trans Mag* (1999) **35**, 4423.
19. Ramesh, R., *Nat Mater* (2010) **9**, 380.
20. Kuemmeth, F., et al., *Mater Today* (2010) **13** (3), 18.
21. Xiu, F., et al., *Nat Mater* (2010) **9**, 337.
22. Moore, J. E., *Nature* (2010) **464**, 194.
23. Dash, S. P., et al., *Nature* (2009) **462**, 491.
24. Dediu, V. A., et al., *Nat Mater* (2009) **8**, 707.
25. Sanvito, S. *Nat Mater* (2007) **6**, 803.
26. Tombros, N., et al., *Nature* (2007) **448**, 571.
27. Houssameddine, D., et al., *Nat Mater* (2007) **6**, 447.
28. Son, Y. -W., et al., *Nature* (2006) **444**, 347.
29. Wolf, S. D., et al., *MRS Bulletin* (2006) **31**, 400.
30. Zutic, I., and Fuhrer, M., *Nat Phys* (2005) **1**, 85.
31. Ralph, D., and Buhrman, R., In: *Concepts in Spintronics* (ed. Maekawa, S.) (2006) Oxford University Press.
32. Myers, E. B., *Science* (1999) **285**, 867.
33. Parkin, S. S. P., et al., *Science* (2008) **320**, 190.
34. Yamada, K., et al., *Nat Mater* (2007) **6**, 270.
35. Lee, K. -S., et al., *Rev Lett* (2008) **101**, 267206.
36. Lee, K. -S., and Kim, S. -K., *Appl Phys Lett* (2007) **91**, 132511.
37. Zhao, T., et al., *Nat Mater* (2006) **5**, 823.
38. Garcia, V., et al., *Science* (2010) **327**, 1106.
39. Fiebig, M., et al., *Nature* (2002) **419**, 818.
40. Hur, N., et al., *Nature* (2004) **429**, 392.
41. Block, T., et al., *J Solid State Chem* (2003) **176**, 646.
42. Elmers, H. J., et al., *Phys Rev B* (2003) **67**, 104412.
43. Felser C., and Hillebrands B., (Guest Editors) *J Phys D: Appl Phys* (2009) **42**, 080301.
44. Klaer, P., et al., *Phys Rev B* (2009) **80**, 144405.
45. Umetsu, R. Y., et al., *J Phys D: Appl Phys* (2010) **43**, 10500.
46. Kubota, T., et al., *Appl Phys Lett* (2009) **95**, 222503.
47. Maekawa, S., *Nat Mater* (2009) **8**, 777.
48. Takahashi, S., and Maekawa, S., *Sci Technol Adv Mat* (2009) **9**, 014105.
49. Yang, T., et al., *Nat Phys* (2008) **4**, 851.
50. Sharma, P., *Science* (2005) **28**, 531.
51. Stern, N. P., et al., *Nat Phys* (2008) **4**, 843.
52. Uchida, K., et al., *Nature* (2008) **455**, 778.
53. Mosendz, O., et al., *Phys Rev B* (2009) **80**, 104439.
54. Mosendz, O., et al., *Phys Rev Lett* (2010) **104**, 046601.
55. Stoehr J., and Siegmann, H. C., *Magnetism*, Springer (2006).
56. Stanciu, C. D., et al., *Phys Rev Lett* (2007) **99**, 047601.
57. Vahaplar, K., et al., *Phys Rev Lett* (2009) **103**, 117201.
58. Kimel, A. V., et al., *Nat Phys* (2009) **5**, 727.
59. Mentink, J. H., et al., *J Phys: Condens Matter* (2010) **22**, 176001.
60. Chen, C. T., et al., *Phys Rev B* (1990) **42**, 7262.
61. Kortright, J. B., et al., *J Mag Magn Mat* (1999) **207**, 7.
62. Stoehr, J., et al., *Science* (1993) **259**, 658.
63. Chao, W., et al., *Nature* (2005) **435**, 1210.
64. Attwood, D. T., *Soft X-rays and Extreme Ultraviolet Radiation: Principles and Applications*, Cambridge University Press (1999).
65. Fischer, P., et al., *Mater Today* (2006) **9**, 26.
66. Fischer, P., et al., *Z.f. Physik B* (1996) **101**, 313.
67. Kortright, J. B., et al., In: Meyer-Ilse, W., Warwick, T., and Attwood, D., (eds.), *X-Ray Microscopy*, American Institute of Physics, Melville (2000) **507**, 49.
68. Chao, W., et al., *Opt Express* (2009) **17** (20), 17669.
69. Barkhausen, H., *Z Phys* (1919) **20**, 401.
70. Ryu, K. -S., et al., *Nat Phys* (2007) **3**, 547.
71. Kim, D. -H., et al., *Phys Rev Lett* (2003) **90**, 87203-1.
72. Sharoni, A., et al., *Phys Rev Lett* (2008) **101**, 026404.
73. Sethna, P., et al., *Nature* (2001) **410**, 242.
74. Field, S., et al., *Phys Rev Lett* (1995) **74**, 1206.
75. Fisher, D. S., *Phys Rev Lett* (1983) **50**, 1486.
76. Im, M. -Y., et al., *Appl Phys Lett* (2009) **95**, 182504.
77. Im, M. -Y., et al., *Adv Mater* (2008) **20**, 1750.
78. Parkin, S. S. P., (2004) US Patent 309,6,834,005.
79. Allwood, D. A. et al, (2005) *Science* **309**, 1688
80. Im, M. -Y., et al, *Phys Rev Lett* (2009) **102**, 147204.
81. Kläui, M., et al., *Phys Rev Lett* (2005) **94**, 106601.
82. Boulle, O., et al., *Phys Rev Lett* (2008) **101**, 216601.
83. Meier, G., et al., *Phys Rev Lett* (2007) **98**, 187202.
84. Bocklage, L., et al., *Phys Rev B* (2008) **78**, 180405(R).
85. Bryan, M. T., et al., *J Appl Phys* (2008) **103**, 07D909.
86. Drews, A., et al., *Appl Phys Lett* (2009) **94**, 062504.
87. Shinjo, T., et al., *Science* (2000) **289**, 930.
88. Wachowiak, A., et al., *Science* (2002) **298**, 577.
89. Miltat, J. and Thiaville, A., *Science* (2002) **298**, 555.
90. Kasai, S., et al., *Phys Rev Lett* (2008) **101**, 237203.
91. Vila-Comamala, J., et al., *Ultramicroscopy* (2009) **109**, 1360.
92. Chao, W., et al., (2010) in preparation.
93. Hellwig, O., et al., *Appl Phys Lett* (2010) **96**, 052511.
94. Ross, C. A. and Cheng, J. Y., *MRS Bulletin* (2008) **33**, 838.
95. Zhu, D., et al., *Phys Rev Lett* (2010) **105**, 043901.
96. Streit-Nierobisch, S., et al., *J Appl Physics* (2009) **106**, 083909.
97. Whitehead, L. W., et al., *Phys Rev Lett* (2009) **103**, 243902.
98. Schneider, J. R., *Nucl Instrum Meth A* (1997) **398**, 41.
99. Tiedtke, K., et al., *New J Phys* (2009) **11**, 023029.
100. La-O-Vorakiat, C., et al., *Phys Rev Lett* (2009) **103**, 257402.
101. Murnane, M. M., et al., *Science* (1991) **251**, 531.